Optical manipulation and study of single gold nanoparticles in solution

Ruijgrok, P.V.

2

Pushing the detection limits of photothermal microscopy

Abstract – We show how to push the detection limits in photothermal microscopy towards weaker single absorbers, by a systematic optimization of signal and noise sources. In particular, we (i) maximize the power of the probe laser beam, (ii) select optimal optical and thermal properties for the medium embedding the absorber, (iii) thermally isolate the absorber from the glass substrate. These different experimental conditions are optimized in turn with single immobilized gold nanoparticles. We demonstrate the detection of a dissipated power of 3 nW with a signal-to-noise ratio of 8, and an integration time of 10 ms. This corresponds to less than 0.1 K surface temperature rise for a 20 nm-diameter gold nanosphere (0.4 K for 5 nm).

The contents of this chapter are based on:
A. Gaiduk, P. V. Ruijgrok, M. Yorulmaz and M. Orrit, "Detection limits in photothermal microscopy", Chem. Sci. **1**, 343-350 (2010)

2.1 Introduction

Photo-thermal, photo-acoustic and photo-optical (photo-refractive and photochromic) effects are widely used in physics, analytical chemistry and medicine.[93] Photothermal spectroscopy is a two-color nonlinear optical technique, in which a heating (pump) beam is absorbed by the species to be detected, causing heat release and a local change of refractive index. The propagation of a second beam at a different wavelength, the probe, will thus be modified by the produced heat. These changes produce the observed signal.[94] Photothermal spectroscopy provides a number of ultra-sensitive methods to measure optical absorbance and estimate concentrations of nanometer-sized particles and non-fluorescent molecules in solvents.[41,95] Photothermal detection has two main advantages. First, the signal is free from background and not sensitive to weak scattering, because the signal only arises from absorbing centers that dissipate heat. Second, because the probe only reacts to refractive index changes, the probe wavelength can be chosen outside of the absorption range of the centers. Therefore, the probe power can be increased to very high values, for which photon noise in the probe detection may become extremely small. The maximum probe power applicable is ultimately limited by sample damage.

Recent developments based on the combination of photothermal effects and interferometric detection have opened up absorption properties of individual labels to optical detection with a high signal-to-noise ratio. Such absorbing labels do not need to fluoresce and have been small ($< 40\,\text{nm}$ diameter) noble metal nanoparticles, quantum dots, or single-walled carbon nanotubes.[43,44,96–101] In contrast to the organic molecules used in fluorescence detection, these labels generally show neither photobleaching nor photoblinking, which makes them attractive for many applications, such as DNA microarrays,[102] gold-labeled protein detection in cells,[103] optical tracking in live cells[104] and high-throughput screening.[105]

Recently, the dynamic range of photothermal microscopy experiments has expanded and new applications have been suggested. Photothermal correlation spectroscopy has been proposed to study the diffusion of single gold nanoparticles in fluid media, and was demonstrated with protein-gold complexes and gold-labeled bacteriophage viruses.[106–108] The selectivity and sensitivity of photothermal detection was demonstrated for direct imaging of mitochondria in live cells, without need for any labeling.[109] The origin of the photothermal contrast of mitochondria is still not well understood, for the abundant inter-membrane protein cytochrome c was excluded as the source

of the photothermal signal. The anisotropic absorption properties of small (25 $\times$ 75 nm) gold nanorods have been probed with polarization-sensitive photothermal microscopy.[110] The authors of that work propose to use plasmon resonances of rods to probe orientation and dynamics of macromolecules in highly scattering environments. A photothermal excitation combined with digital heterodyne holography[111] provides wide-field (up to 100 μm^2 area) photothermal detection of 50 nm and smaller gold particles. The method involves a trade-off between large observation areas, video rate acquisition speed, and a large radius of heat diffusion.[112] Compared to single-point detection, the signal-to-noise of wide-field detection is about an order of magnitude lower.

To further expand the performance and applications of single-point photothermal detection, it is important to look for its detection limits. To our knowledge, the best signal-to-noise ratio measured in single-point photothermal detection[97] was about 10 for a 5 nm gold nanoparticle (NP) heated with a power of 500 μW (514 nm), with unspecified probe power, and with an integration time of 10 ms.[†] We estimate the absorbed power in these experiments to 20 nW. It is important to know how far this result is from the theoretical limit.[100,106] In the several publications following this early work, little attention has been paid to the various factors which may influence the signal-to-noise ratio in photothermal detection.

In this Chapter, we examine how the probe power, the thermal properties of the medium, and thermal isolation of the absorber from the glass substrate influence the signal-to-noise ratio in photothermal detection.

2.2 Method

Photothermal detection is sensitive to the amount of energy absorbed by a nanoobject and dissipated as heat into its local environment. We define as the dissipated power P_{diss} the power provided by a heating beam (with power P_{heat}), which is dissipated as heat by the absorber. Because the heating beam intensity is modulated at an angular frequency Ω , we call P_{diss} the maximum instantaneous value of this power during the modulation period. The time-averaged dissipated power is therefore $P_{\text{diss}}/2$. For a spherical gold particle

[†]The same group reported detection of gold NP as small as 1.4 nm (67 atoms) with a signal-to-noise ratio of about 10, achieved with integration of 10 ms and a temperature rise of $\sim$2 K.[44] However, some of the parameters of the experiment are unspecified. Our calculation of the dissipated power for these particles in these conditions is 4 nW

of radius R placed in a homogeneous medium with thermal conductivity κ, the maximum temperature increase $\Delta T(r,t) = \Delta T_{\text{surf}}$ scales as R^2, because the cross-section σ_{abs} scales as R^3.[6,49,113] The thermal radius $r_{\text{th}} = \sqrt{2\kappa/\Omega C_{\text{p}}}$ is the characteristic length of heat diffusion in the medium, where C_p is the heat capacity per unit volume of the photothermal medium. Dissipation of the absorbed energy into the medium results in a temperature profile $\Delta T(r,t)$, which in steady conditions with sinusoidal modulation is given by:[43]

$$\Delta T(r,t) = \frac{P_{\text{diss}}}{4\pi\kappa r}[1 + \exp(-r/r_{\text{th}})\cos(\Omega t - r/r_{\text{th}})] \tag{2.1}$$

Assuming the response to be instantaneous, this temperature profile in turn causes a refractive index profile $\Delta n(r,t) = \Delta T(r,t)\partial n/\partial T$ in the medium, acting as a modulated thermal nanolens.[94] A probe beam is used to detect that nanolens. In the usual photothermal geometry[44,94,95] the scattered probe field $E_{\text{sc}}(t)$ interferes with a reference probe field E_{ref} (usually the transmitted beam or a reflection), and the resulting intensity $I_{\text{det}} \propto |\vec{E}_{\text{ref}} + \vec{E}_{\text{sc}}|^2$ is detected. In this discussion, we neglect the difference in spatial modes of the two fields, which are supposed to be similar. The lock-in amplifier filters out the weak contribution to the interference signal $2\text{Re}[\text{E}^*_{\text{ref}}\text{E}_{\text{sc}}]$ modulated at the same frequency as the heating beam. The contribution of the modulated scattered intensity $|\vec{E}_{\text{sc}}|^2$ is neglected for small particles (typically $< 60\,\text{nm}$ diameter).[49] For larger particles, a non-negligible static scattered field acts as an additional in-phase reference field. Its contribution to the interference intensity I_{det} is reported in photothermal correlation spectroscopy experiments for 80 nm diameter gold particles.[106] The photothermal signal S is proportional to the field scattered by an effective volume V where the refractive index is modulated. The refractive index change Δn depends on the absorption cross-section σ_{abs} of the nanoobject and the heating beam with intensity I_{heat} focused into a diffraction-limited spot with area A. Δn is proportional to the power dissipated by the nanoobject $P_{\text{diss}} = I_{\text{heat}}\sigma_{\text{abs}} = \sigma_{\text{abs}}P_{\text{heat}}/A$. The field scattered by the thermal lens can be approximated by that of an equivalent dipole $|\vec{p}| \approx 2n\Delta n \cdot V|\vec{E}_{\text{probe}}|$, where $\Delta n \cdot V$ stands for the volume integral of the position-dependent refractive index change of the lens. The scattered field is radiated by this dipole: $|\vec{E}_{\text{sc}}(t)| \approx |\vec{p}|/(4\pi\epsilon_0\omega_0\lambda^2)$, and the photothermal signal can then be written as an optical power:

$$S \approx \frac{1}{\pi\omega_0} n \frac{\partial n}{\partial T} \frac{1}{C_p\lambda^2\Omega} \frac{\sigma_{\text{abs}}}{A} P_{\text{heat}}P_{\text{probe}}\Delta t \tag{2.2}$$

where ω_0 is the probe beam focal radius (beam waist), λ and P_{probe} are the wavelength and power of the probe beam, and Δt is the integration time of

the lock-in amplifier. We assume the thermal conductivity of metal nanoparticles to be much larger than that of the surrounding media (for example, $\kappa_{\text{gold}} = 310\,\text{W}\,\text{m}^{-1}\,\text{K}^{-1}$, $\kappa_{\text{water}} = 0.6\,\text{W}\,\text{m}^{-1}\,\text{K}^{-1}$).

The noise in actual experiments arises from the detector, from fluctuations of the probe laser power, and from photon noise of the detected optical power. In practice, the experimental noise is always larger than the photon noise, but can be close to it for an optimized setup. Here, assuming an ideal detector and a shot-noise limited detection, the noise on the photothermal signal N would be:

$$N \propto \sqrt{\frac{P_{\text{probe}}\Delta t}{h\nu}} \tag{2.3}$$

where h is Plank's constant and ν is the frequency of the probe light. Combining the expressions for the signal and the noise, we see that the signal-to-noise ratio SNR for the shot-noise-limited photothermal detection is given by:

$$SNR \approx \frac{1}{\pi\omega_0\lambda^2\Omega} n \frac{\partial n}{\partial T} \frac{1}{C_p} \frac{\sigma_{\text{abs}}}{A} P_{\text{heat}} \sqrt{\frac{P_{\text{probe}}\Delta t}{h\nu}} \tag{2.4}$$

We now discuss how the SNR can be optimized by tuning all factors in Eq. 2.4, and the practical limits to optimization.

1. Increase the dissipated power up to the allowed maximum, usually fixed by saturation. For gold nanoparticles, the applicable powers are very high (the bulk melting temperature of gold is about 1300 K, and the temperature rise to reshape gold nanorods, although significantly lower[114,115] is still some hundreds of K). The allowed temperatures in biological samples, however, will be much lower. The melting intensity for a spherical particle with diameter 20 nm in water is around $20\,\text{MW}/\text{cm}^2$ at 514 nm (about 20 mW focused on a spot), and scales with R^2. For a non-fluorescent molecule, the saturation intensity is determined mostly by the excited state lifetime τ, typically 0.1 ns, which leads to a dissipated power of a few nW.

2. Increase P_{probe} as much as possible. Practical limits are set by the maximum available laser power and by residual absorption of the probe beam by the sample. For example, the probe power can be increased until the probe-induced and pump-induced heating are comparable. For small gold NPs in glycerol, for example, we can use up to 170 times more probe power at 800 nm than heating power at 532 nm, as given by the ratio of the absorption cross-sections.

3. Match the heat diffusion length r_{th} with the spot size, by choosing the right modulation frequency Ω.[43,100] A lower modulation frequency generally leads to a higher photothermal signal, until the thermal lens exceeds the size of the focused probe beam. The optimal value of the modulation frequency also depends on the experimental noise spectrum.

4. Optimize the optical and thermal properties of the photothermal medium, including refractive index, its derivative with respect to temperature, heat capacity and conductivity (see Section 2.5.2 and Appendix A).

5. Increase the integration time of the lock-in amplifier. This parameter can be increased arbitrarily, provided the mechanical stability of the experimental setup and the photostability of a sample allow it.

2.3 Experimental

2.3.1 Sample preparation

Samples of gold colloids with diameters of 5 nm and 20 nm (British Biocell International, EM.GC5 and EM.GC20) were prepared by dilution in ultrapure water at the ratios of 1:40 and 1:8, respectively. Approximately 50 μL of the suspension were deposited on the surface immediately after the filtration through a 450 nm porous membrane and spin coated at 2000 rpm for 5 s, followed by drying at 4000 rpm for 90 sec. Glass coverslides (Menzel, Germany) were cleaned by sonication for 20 min in the following solvents: 2 % Hellmanex (Hellma) solution in water, acetone (96% purity), ethanol (96% purity). Additional sonication in water was performed prior to each cleaning step. The glass coverslides were then dried and treated in a UV-ozone cleaner for at least 30 min prior to following sample preparation steps. PMMA, poly(methyl-methacrylate) with M_W = 96.7 kDa (Sigma-Aldrich) was used to prepare a thermal isolation layer on top of clean substrates. About 50 μL of PMMA solution in toluene at 30 g/L concentration was spin coated. The thickness of the resulting PMMA layer was measured by AFM and found to be 100-120 nm. For preparation of nanoparticles (NP) on PMMA, a 2 % PVA solution (polyvinyl alcohol, M_W = 130 kDa, Fluka) in water was mixed with NPs to provide the desired concentrations of gold colloids and 1 % concentration of PVA. The sample was prepared via spin coating, resulting in PVA layer thickness of approximately 20 nm. The thin PVA film was found

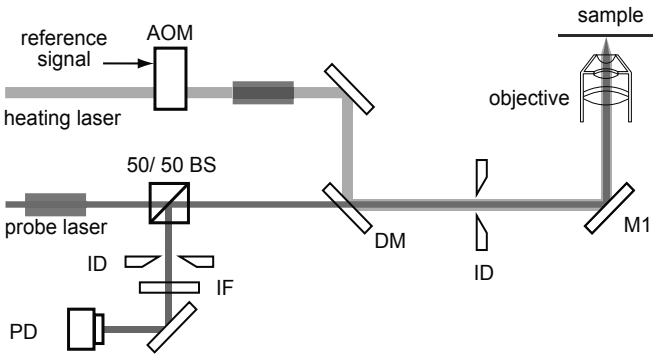

Figure 2.1: Scheme of the experimental setup for simultaneous photothermal and fluorescence detection. The heating light for photothermal microscopy also excites fluorescence at the same time. AOM - acousto-optical modulator, M - mirror, BS - beam splitter, DM - dichroic mirror, ID - iris diaphragm, IF - interference filters, APD - avalanche photodetector, PD - photodiode. Polarizer, spatial filters are not shown in this scheme. Grey boxes schematically indicate the positions of the telescopes and beam expander.

to be dissolved after several hours in glycerol. NPs remain adsorbed on the PMMA surface. The measurements were performed in a fluid cell with $\sim$ 50 μL photothermal medium. The cell was assembled from two glass coverslips and a rubber o-ring attached to the bottom one. Clean glycerol (>99.5%, spectrophotometric grade), ethanol (spectroscopy grade), chloroform (spectroscopy grade), dichloromethane, pentane, and hexane (all AR grade) were used as photothermal media.

2.3.2 Photothermal detection setup

The experimental setup is based on a home-built microscope equipped with an Olympus 60$\times$ oil immersion objective (NA = 1.4 or NA = 1.45) and is sketched in Fig. 2.1. The heating beam is provided by either a laser diode at 532 nm (Shanghai Lasers, power 150 mW) or by an Ar-ion laser (Coherent, max. output 10 W). The heating light passes an acousto-optical modulator (AOM) which is operated typically at Ω = 740 kHz. The beam is expanded in a spatial filter (60 mm and 100 mm lenses, with a 30 μm pinhole,) and a telescope (100 mm and 200 mm) to about 20 mm, and overfills the entrance pupil of the microscope objective (approximately 10 mm). The expanded beam is sent towards the microscope objective by a dichroic mirror (BS 669, AHF) on which heating and probe beams are combined. The probe beam at 790 nm

or 800 nm is provided by a Ti:sapphire laser (either Mira, Coherent, pumped with Coherent Verdi V10; or Spectra Physics, 3900 S, pumped by 90% of the power of the Ar-ion laser). The near-infrared light (NIR) passes a polarizer and a spatial filter (two 75 mm lenses with a 30 μm pinhole). A variable beam expander 2-5$\times$ provides the continuous adjustment of the diameter of the probe light to ensure the optimal overfilling of the objective lens with the desired probe power. A 50/50 beam splitter (Halle) is used to reflect half the power of the probe laser to the microscope and transmit half the back-scattered probe light towards the detector. The spectrally filtered probe light is focused with a 100 mm lens onto a photodiode (Femto DHPCA-100-F, Germany) or optionally monitored by a CCD camera (Ganz, Germany). A wave generator (33250A, Agilent) provides the modulation signal for the AOM and the reference of the lock-in amplifier (SR844, Stanford Research Systems) analyzing the photodiode output. All data acquisition and processing is performed by an acquisition card (ADWin Gold, Germany) linked to a computer. The sample is scanned with a 3-axis piezostage (NanoCube, Physik Instrumente).

2.4 Photothermal imaging of gold nanoparticles

We first demonstrate the performance of our setup with photothermal microscopy on 5 nm and 20 nm diameter gold nanoparticles. A photothermal microscopy image (Fig. 2.2 A) shows about 30 particles with 20 nm diameter (density $<$1 NP/μm^2) and 3 particles with 5 nm diameter (density $<$0.1 NP/μm^2). Cross-sections of the spots of some 20 nm NP and of the 5 nm NP indicate an intensity ratio of 35, not too far from the expected ratio $(20/5)^3 = 64$ (Fig. 2.2 B). The difference is explained by deviations from the nominal average NP diameter provided by the manufacturer. Indeed, we found by AFM and SEM that the diameters of the nominal 20 nm NPs varied between 14 nm and 18 nm. Moreover, some particles, for example triangles, were found to deviate significantly from the spherical shape. The results of the photothermal imaging and SNR analysis of 73 particles of 20 nm and 119 particles of 5 nm are presented in Fig. 2.2 C and summarized in Table 2.1.

We detect 20 nm NPs with a SNR of 420 and an integration time of 1 ms with 260 μW of heating power and 20 mW of probing power at the sample's position. These values correspond to 810 nW of dissipated heating power and to 170 nW of dissipated probe power. The total power absorbed corresponds to a temperature rise of about 28 K at the surface of a 20 nm NP. A SNR of

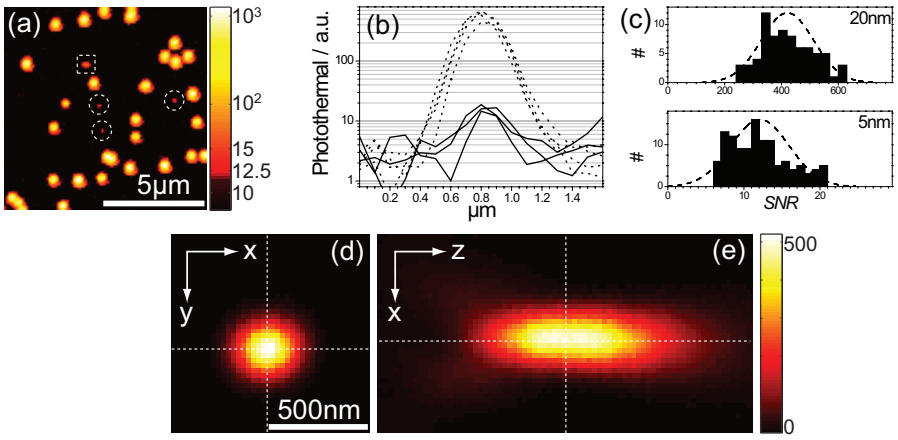

Figure 2.2: a) Photothermal microscopy image of a sample with gold nanoparticles of 20 nm and 5 nm diameter immobilized on a glass slide in glycerol. The photothermal signal is color-coded on a logarithmic scale. Circles mark the positions of 5 nm NPs. The NP in the square box may be an aggregate. P_{heat} = 0.26 mW, P_{probe} = 20 mW, Δt = 1 ms, $T_{\text{surf}} \sim 28$ K. (b) Several cross-sections of 20 nm (dashed lines) and 5 nm (solid lines) NP along the slow scan axis (horizontal in the image) present relative signals for particles of different sizes. (c) Histograms of the photothermal SNRs for gold NP of 20 nm (top, 73 NP) and 5 nm (bottom, 119 NP). The population of 5 nm particles has $SNR = 12 \pm 4$, while the population of 20 nm particles has $SNR = 421 \pm 92$. Experimental data are presented in histograms. (d) Photothermal image of a single 20 nm gold colloid. (e) Photothermal image of a single 20 nm gold NP taken along the vertical z-axis, perpendicular to the glass surface. Gaussian fits of the shape of the signal along the z-, y- and x-axes gives FWHM values of 730 nm, 250 nm, and 220 nm, respectively. Vertical dashed lines indicate the position of the glass-glycerol interface (glass on the right-hand side).

12 is achieved with the same integration time, heating, and probe powers for 5 nm NPs. For the 5 nm particles, the dissipated powers are 12.6 nW for the heating beam and 2.6 nW for the probing beam, and the respective surface temperature rise about 0.5 K. The spatial overlap of heat and probe beam in photothermal microscopy provides optical sectioning and defines the spatial resolution. The photothermal detection volume is defined by the product of the point spread functions of heating and probe beams. By focusing both beams into overlapped diffraction-limited spots, we achieve a lateral spatial resolution of about 240 nm, and an axial resolution of 730 nm (Fig. 2.2 D,C).

Table 2.1: Experimentally obtained signal-to-noise ratios (SNR) in photothermal detection of gold nanoparticles on glass in glycerol [a]

Diameter	$P_{\mathrm{diss}}^{\mathrm{pump}}$ (nW)	$P_{\mathrm{diss}}^{\mathrm{probe}}$ (nW)	$\Delta T_{\mathrm{surf}}^{\mathrm{pump}}$ (K)	$\Delta T_{\mathrm{surf}}^{\mathrm{probe}}$ (K)	SNR
20 nm	810	170	23	4.8	421
5 nm	12.6	2.6	0.4	0.08	12

[a] Heating with 532 nm ($I_{\mathrm{heat}} = 130\,\mathrm{kW\,cm^{-2}}$), probing with 790 nm ($I_{\mathrm{probe}} = 4.5\,\mathrm{MW\,cm^{-2}}$). Integration time Δt is 1 ms. $P_{\mathrm{diss}}^{\mathrm{pump}}$ $\left(P_{\mathrm{diss}}^{\mathrm{probe}}\right)$ and $\Delta T_{\mathrm{surf}}^{\mathrm{pump}}$ $\left(\Delta T_{\mathrm{surf}}^{\mathrm{probe}}\right)$ are the dissipated power due to the pump (probe) laser and the corresponding particle surface temperature, respectively.

2.5 Improvements of SNR in photothermal detection of gold NP

Hereafter, we discuss several possible ways to increase the photothermal SNR, and verify them experimentally with 20 nm gold NPs.

2.5.1 Reduce photon noise with higher probe powers

As follows from Eq. 2.4, the SNR in ideal photothermal experiments should be proportional to the square root of the probe power. The measurements of SNR are presented in Fig. 2.3 A. The good agreement with the expected power law (Eq. 2.4) indicates that the noise in our photothermal detection is mainly determined by photon noise. In particular, for the range of probe powers detected in our experiments, laser noise is negligible. At low probe powers, the SNR deviates from the square-root dependence because of detector noise, which is independent of power. To achieve maximum sensitivity in the photothermal detection, we want to keep the photodetector gain maximal. This gain is limited by the total power reaching the detector. Apart from its weak time-dependent component encoding the photothermal signal, the detected probe power has a strong static contribution, which arises from reflection by the glass-liquid interface. The reflected power, determined by the refractive index mismatch between the BK7 glass (n = 1.52) and the medium, varies from $4.4\,10^{-3}$ for the glass-water (n = 1.33) to $2.5\,10^{-4}$ for the glass-glycerol (n = 1.473) interfaces, as given by Fresnel's equations for normal incidence. We chose a maximum detected probe power of 18 μW, corresponding to a gain of 10^5 A/V, which is a trade-off between high probe power and low photodetector noise. Then, the maximal incident probe power varies from

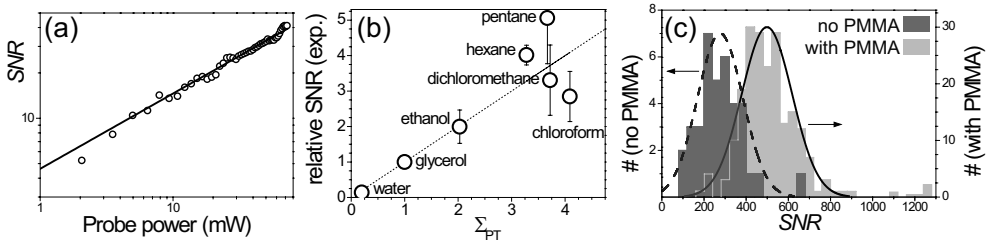

Figure 2.3: (a) Photothermal signal-to-noise ratio as a function of the incident probe power ($\lambda = 790$ nm) measured for 20 nm gold NPs in water on glass. The fit shows the square root dependency of the SNR. (b) Photothermal SNR measured for 20 nm NPs in different fluids as a function of calculated photothermal strength for these fluids Σ_{PT} , scaled with respect to glycerol. Measurements were done on a few NPs in water, 116 NPs in glycerol, 92 NPs in ethanol, 60 NPs in dichloromethane, 41 NPs in hexane, 63 NPs in chloroform and 30 NPs in pentane. The error bars give the standard deviation of the distribution. (c) Normalized histograms of SNR for 20 nm gold NP in glycerol: (dark grey) deposited on glass, $SNR = 272 \pm 110$ over 38 particles; (light grey) deposited on a 100 nm thick thermal isolation layer of PMMA, $SNR = 502 \pm 128$ over 211 particles. Among them, 6 particles show SNR values twice the mean distribution value (>1000) indicating a few aggregates (<3%) in the area of 1000 μm^2. Experimental parameters: heating with 0.27 mW incident power at 514 nm, probe at 800 nm with 23 mW incident power, corresponding to a total T_{surf} $\sim$ 28 K (due to heat and probe), integration time 3 ms

4 mW for water to 72 mW for glycerol. Note that achieving photon-noise limited detection in the forward direction is more difficult than in the backward direction for two reasons. First, it is difficult to find fast and sensitive detectors for powers larger than 20 mW. Second, photon-noise limited detection of higher powers requires a lower laser noise.

2.5.2 Solvent

As has been known for many years, the thermal properties of the solvent are crucial for photothermal spectroscopy and its applications to analytical chemistry.[94] An obvious step to enhance the photothermal signal is to select a solvent with a high sensitivity of its refractive index to a temperature change, ($\partial n/\partial T$). Note, however, that this (usually negative) quantity is only a crude figure of merit characterization of the heating-induced change of refraction for small enough temperature raises. To account for the full space- and time-dependent changes of refractions around the heated object, the full

function $n(r,T)$ should be considered. In addition to its optical properties, the thermal properties of a medium determine the magnitude of the photothermal signal. We selected several organic fluids based on their expected value for a parameter we call 'photothermal strength' (See Appendix A):

$$\Sigma_{\mathrm{PT}} = n \left| \frac{\partial n}{\partial T} \right| \frac{1}{C_p}. \tag{2.5}$$

This parameter characterizes the refractive index change that is produced by a given energy density (heat/unit volume) stored in the photothermal medium. However, because the thermal radius r_{th} must be fixed in relation to the probe wavelength, it may be more physical to define an alternative figure of merit of photothermal media FOM:

$$FOM = n \left| \frac{\partial n}{\partial T} \frac{1}{\kappa} \right|, \tag{2.6}$$

which is equivalent to $\Sigma_{\mathrm{PT}}/r_{\mathrm{th}}^2$. These two characterizations do not differ much in their predictions for selected fluids. We have measured the photothermal signals of 20 nm NPs in equivalent conditions. The results are presented in Fig. 2.3 B and correlated with the expected photothermal strength Σ_{PT}. The agreement with the expected signal is only approximate for the highest photothermal strengths. As indicated, the SNR can be improved by up to 5 times by performing experiments in pentane, as compared to glycerol. Glycerol itself gives 5 times higher SNR than water at 20 °C. Clearly, fluid media with a large sensitivity of their refractive index to temperature (large thermal expansion coefficients) will be interesting for photothermal detection. These are fluids close to their critical points or to phase transitions, as well as mixtures close to demixing points, presenting a large Soret effect. However, the temporal response of a medium is slowed down dramatically close to a critical point, and the sensitivity only appears in a small temperature range close to the critical point. For strong heating, the enhancement of the refractive response would be essentially destroyed by averaging over space and time.

2.5.3 Thermal isolation

The thermal conductivity of glass ($1.05\,\mathrm{W\,m^{-1}\,K^{-1}}$) is more than 3 times larger than that of most organic liquids ($0.28\,\mathrm{W\,m^{-1}\,K^{-1}}$ for glycerol). Therefore, a large part of the generated heat will be lost to glass, where the associated

refractive index change is very small. The thermal conductivity of the glass support, which acts as a heat sink, thus reduces the photothermal effect. A thermal isolation layer introduced between the absorber and its solid substrate will reduce the 'leak' of heat into the glass. We chose to prepare a thin PMMA film (heat conductivity $0.2\,\mathrm{W\,m^{-1}\,K^{-1}}$) on the top of glass substrate prior to gold NP deposition. The film deposited via spin coating was found by AFM measurements to have a homogeneous thickness of 100-120 nm. An alternative way to achieve thermal isolation is to use a PMMA substrate, however available substrates have poor optical quality and are too thick compared to the working distance of high NA microscope objectives. A comparison of photothermal SNR for 20 nm gold particles on glass and on PMMA on glass, both in glycerol, is shown in Fig. 2.3 C. We demonstrate a signal increase by 1.8 times in the presence of the thermal isolation layer, as measured on 38 NPs on glass and 211 NPs on PMMA on glass. This number is smaller than 4, the expected ratio of heat leaks based on the assumption of a perfect isolation. Heat diffusion simulations in this complex geometry would be needed for a more quantitative comparison.

2.6 Smallest detectable dissipated power in photothermal detection

To compare the efficiencies of photothermal detection of different point-like objects in different conditions, it is sufficient to compare the powers P_{diss} they dissipate in their environment. In the following, we probe the limits of photothermal detection in experiments with 20 nm gold NPs in glycerol, which serve as test objects with a well-defined absorption cross-section. We experimentally estimate the smallest P_{diss} and temperature rise T_{surf} which we can detect with a reasonable SNR. Typical results for the photothermal detection of dissipated powers down to 2.6 nW on glass and in glycerol are demonstrated in Fig. 2.4. Here, heating powers of $9\,\mu$W (Fig. 2.4 A) and $1\,\mu$W (Fig. 2.4 B) at 514 nm were used. The dissipated powers were 24 nW (Fig. 2.4 A) and 2.6 nW (Fig. 2.4 B) corresponding to temperature rises of 0.7 K (A) and 80 mK (B). These are detected with an average $SNR = 20$, with a 3 ms integration time (Fig 2.4 A), and $SNR = 8$, with a 10 ms integration time (Fig 2.4 B).

According to our previous discussion, there are several ways to increase the SNR compared to Fig. 2.4. We can win a factor of 2 by increasing P_{probe} from 68 mW to 280 mW. Another factor of 10 can be gained by increasing the

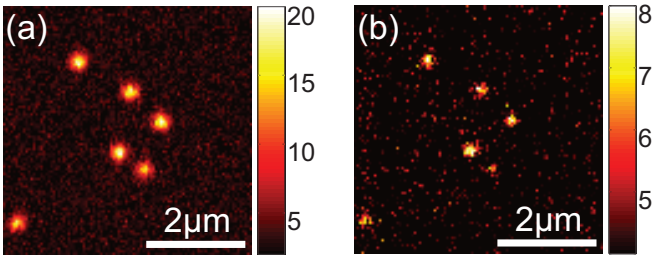

Figure 2.4: Photothermal images of 20 nm gold NPs in glycerol with (a) $P_{\text{heat}} = 9\,\mu$W, $P_{\text{probe}} = 23$ mW, $\Delta t = 3$ ms, and with (b) $P_{\text{heat}} = 1\,\mu$W,$P_{\text{probe}} = 68$ mW, $\Delta t = 3$ ms. Dissipated powers (P_{diss}) and temperature rises (T_{surf}) are 24 nW and 2.6 nW, and 0.7 K and 80 mK, with average SNR of 20 and 8, respectively. Heating and probing wavelengths 514 nm and 800 nm.

integration time of the lock-in amplifier (Δt) from 10 ms to 1 s. A further enhancement factor of 5 can be gained with a better photothermal medium (pentane instead of glycerol), and one of about 2 with thermal isolation of the particle from the substrate (with PMMA layer). Overall, the SNR can be increased by a factor of 200. Thus, with the achieved sensitivity and proposed experimental conditions we would be able to detect dissipated powers lower than 15 pW within 1 s, with a SNR of 8.

2.7 Conclusions

We have proposed several ways to increase the signal-to-noise in photothermal detection. We demonstrate that (i) our SNR is very close to limited by photon noise, in particular laser noise is negligible, (ii) the choice of photothermal medium is very important to achieve a high sensitivity (e.g., pentane gives a 5 times higher signal than glycerol), (iii) a significant signal increase can be achieved by introducing a thin layer of polymer between the glass substrate and the photothermal medium (here, 100 nm of PMMA led to an improvement of the signal by a factor of about 2). The sensitivity of photothermal detection can further be improved by (i) better focusing of the heat and probe beams (for example using radially polarized light[116] or immersion in higher indices[117]); (ii) using a photothermal medium with even larger refractive index changes with temperature, for example fluids close to phase transitions. Furthermore, we have demonstrated the photothermal detection of 3 nW of dissipated power with a SNR $\sim$8 in 10 ms.

Acknowledgments

We thank Anna Pezzarossa and Prof. Thomas Schmidt for help with wide-field fluorescence microscope, BioAFM lab for providing access to AFM, and Peter Zijlstra for SEM images of gold NP.